Robust Adaptive Segmentation of Range Images

Kil-Moo Lee, *Member, IEEE*, Peter Meer,* *Senior Member, IEEE*

Rae-Hong Park, *Member, IEEE*

Department of Electronic Engineering, Sogang University

C.P.O. Box 1142, Seoul 100-611, Korea

lkm@eevision1.sogang.ac.kr, rhpark@ccs.sogang.ac.kr

*Department of Electrical and Computer Engineering

Rutgers University, Piscataway, NJ 08855, USA

meer@caip.rutgers.edu

Correspondence to:

Prof. Rae-Hong Park

Dept. of Electronic Eng., Sogang University

C.P.O. Box 1142, Seoul 100-611, Korea

Tel : 82-2-705-8463

Fax : 82-2-705-8629

e-mail : *rhpark@ccs.sogang.ac.kr*

Abstract

We propose a novel image segmentation technique using the robust, adaptive least k-th order squares (ALKS) estimator which minimizes the k-th order statistics of the squared of residuals. The optimal value of k is determined from the data and the procedure detects the homogeneous surface patch representing the relative majority of the pixels. The ALKS shows a better tolerance to structured outliers than other recently proposed similar techniques: Minimize the Probability of Randomness (MINPRAN) and Residual Consensus (RESC). The performance of the new, fully autonomous, range image segmentation algorithm is compared to several other methods.

Index Terms—**robust methods, range image segmentation, surface fitting**

1 Introduction

A range image provides geometric information about the object independent of the position, direction, and intensity of light sources illuminating the scene, or of the reflectance properties of that object. Many object recognition algorithms using range images as input were proposed [1]. To recognize a 3D object, first its range image has to be segmented into homogeneous regions. Uncorrupted range images can be approximated reasonably well by a piecewise polynomial surface, and thus a homogeneous region corresponds to a polynomial surface patch.

There are two "traditional" approaches toward segmentation of piecewise polynomial data. In the *region-based* range image segmentation methods first the pixels having similar properties are grouped together. For example, Besl [2] classified the pixels as belonging to one of eight surface types depending on the sign of the Gaussian and mean curvature. The range image was then segmented using a variable-order surface fitting algorithm. In the *edge-based* methods,

on the other hand, first the discontinuities are extracted and the segmentation is then guided by the obtained contours. For example, Fan *et al.* [5] extracted edges based on the principal curvature and segmented the image using a heuristic post-processing.

Significant effort is required to compare the performance of different range segmentation methods. In [8] a rigorous framework was developed (including ground truth based quantitative measures) and four traditional techniques for segmentation into planar patches were evaluated. None of the methods provided superior performance under all the evaluation criteria.

Robust estimation techniques [12] can also be used to recover the parameters of a surface patch. The percentage of tolerated outliers determines the breakdown point of the estimator. The two most frequently used classes of robust estimators are the M-estimators and the family of high breakdown point (close to 0.5) techniques. The least median of squares (LMedS) estimator is the best known from the latter class. See [18] for an introductory text on robust estimators with an emphasis on LMedS. The breakdown point of the M-estimators cannot exceed for arbitrary sparse range data 0.3, however, for most noise processes corrupting the inliers the M-estimators being a weighted least squares type technique with data dependent weights, are more efficient than LMedS.

Koivunen and Pietikäinen [10] compared the performance of M-estimators (the algorithm proposed in [3]), and least trimmed squares estimator (a high breakdown point technique). Roth and Levine [20] proposed a Hough transform type evidence accumulation method, similar with the computation of LMedS. The idea of using subsets of the data is also at the basis of the Residual Consensus method proposed by Yu *et al.* [23]. Boyer *et al.* [4] developed a range segmentation system in which an M-estimator is used as the main computational module. The error norm used in [11] provides bounded sensitivity to outliers, i.e., the method can also be regarded as a robust approach.

The breakdown point of any one-step robust estimator cannot exceed 0.5. That is, the inliers must be the absolute majority in the data in order to be able to recover for *arbitrary*

outliers and *without additional assumptions*, their underlying model. This condition cannot be satisfied in a range image, and many segmentation algorithms therefore start by detecting *seed* regions. The homogeneity of the seed regions is established with high confidence, and the final segmentation is obtained by extending these regions using robust estimators and/or heuristics e.g., [4], [11].

However, it is possible to design multi-step procedures which can recover, in the lack of any a priori information, the model parameters representing the *relative* majority of homogeneous pixels in the window of analysis. These procedures tolerate more than half of the data being outliers, i.e., the apparent breakdown point exceeds 0.5. It must be emphasized that this breakdown point does not have the same meaning as that of a one-step robust estimator, i.e., as it is used in statistics.

In Section 2 we propose a multi-step procedure, the adaptive least k-th order squares (ALKS) estimator, and compare its performance with two other procedures described in the literature: Minimization of the Probability of Randomness (MINPRAN) [22], and Residual Consensus (RESC) [23]. In Section 3, a range image segmentation technique based on ALKS is described and its performance compared with several other methods.

2 Adaptive Least k-th Order Square Estimator

Let $r_i,\ i = 1, \cdots, n;$ be the residuals associated with the data points in the window, i.e., the difference between the given observation and the value predicted by the estimated model. (For convenience we use a single index for the data points.) The least median of squares estimator (LMedS) finds the model parameters which minimize $(r^2)_{k:n}$, where the subscript means the k-th largest residual in the ascendingly ordered list, and k is equal to $[n/2] + [(p+1)/2]$ ($[\cdot]$ is the integer part operator), with p being the number of parameters of the model ([18], p.124). The LMedS estimator will always return a model representing at least 50 percent of the data

points.

In the Random Sample Consensus (RANSAC) method [6] (very similar to LMedS though developed earlier [12]) a model is validated by yielding more residuals within a predetermined tolerance band than a cardinality threshold. Through setting the width of the tolerance band and the lower bound on the number of points within it, the user can optimize performance. Stewart [22] generalized the principle behind RANSAC. He assumed that the outliers are uniformly distributed and, for a given tolerance band, the estimated model is the one which yields the least uniformly distributed residuals within. The Minimize the Probability of Randomness (MINPRAN) technique searches across the joint space of tolerance band width and the number of points it can contain.

Like all high breakdown point estimation methods, the Residual Consensus (RESC) method [23] also starts with randomly selecting the minimal number of data points from which the model parameters can be computed. The residuals relative to the model are computed for all the data points and the inliers are selected based on Gaussian noise assumption. The compressed histogram of the inliers' residuals is then used to derive a criterion which is biased toward increased number of inliers with small residuals. The criterion incorporates two user defined parameters.

Adaptively selecting the point set of the relative homogeneous majority, however, can also be achieved with the help of a robust estimator. The least k-th order squares (LKS) uses an arbitrary $p < k < n$ in the minimization and belongs to the family of least quantile of squares estimators ([18], p.124). Taking into account both the explosion and the implosion definitions of the breakdown point [19], we obtain that the LKS estimator has the theoretical breakdown point of $\min\left(\frac{k}{n}, 1 - \frac{k}{n}\right)$.

The computation of LKS is similar to the well-known technique for LMedS (e.g., [12], [18]). A p-tuple is chosen randomly from the data to define a model hypothesis. Using all the computed model parameters except the intercept, the residuals of this partial model, u_i are

computed. The residuals are then sorted in ascending order and the location of the shortest window containing at least k residuals is found. Let

$$d_{l,k} = \frac{u_{(l+k-1):(n-p)} - u_{l:(n-p)}}{2} \tag{1}$$

be the half-width of the corresponding window. The procedure is repeated for several p-tuples. Their number can be established based on simple probabilistic considerations ([18], p.197). The p-tuple yielding the smallest $d_{l,k}$, denoted $\hat{d}_k$, provides the LKS estimate of the model.

The standard deviation of the noise corrupting the inliers, i.e., the *robust* estimate of the noise variance can be approximated as

$$\hat{s}_k = \frac{\hat{d}_k}{\Phi^{-1}[0.5(1+k/n)]} \tag{2}$$

where the compensation factor in the denominator assumes Gaussian distribution for the inlier noise, and $\Phi^{-1}[\cdot]$ is the argument of the normal cumulative density function having the value inside the bracket. The normality of the inlier distribution is not a necessary condition, a rough estimate of how the compensation factor depends on k suffices. Because of the finite sample size n, the compensation factor is not valid for very small, or very large (close to n) values of k. Once $\hat{s}_k$ is determined the inliers are discriminated as having residuals $|r_{i,k}| \leq 2.5\hat{s}_k$.

The optimum value of k must be derived from the data. For any given k the variance of the *normalized error*, ϵ_k^2, is computed

$$\epsilon_k^2 = \frac{1}{q_k - p}\sum_{i=1}^{q_k}\left(\frac{r_{i,k}}{\hat{s}_k}\right)^2 = \frac{1}{\hat{s}_k^2}\frac{\sum_{i=1}^{q_k} r_{i,k}^2}{q_k - p} = \frac{\hat{\sigma}_k^2}{\hat{s}_k^2}\ , \tag{3}$$

where only the residuals of the q_k points declared inliers by the LKS estimator are used. The optimum value of k is chosen as the one yielding the smallest ϵ_k^2. Note that the inliers are selected based on $\hat{s}_k$, and therefore the distribution of ϵ_k^2 is difficult to determine even for the ideal case, homogeneous data corrupted with Gaussian noise. The adaptive procedure using LKS with k chosen by minimizing (3), will be referred to in the sequel as ALKS.

To analyze the behavior of the selection criterion (3) assume first that the data is homogeneous, i.e., all the n data points belong to the same homogeneous patch corrupted with i.i.d. zero-mean noise having standard deviation σ. The robust estimate $\hat{s}_k$ is then an underestimate of σ for all values of k. This observation (supported by extensive simulations) agrees with the remark of Rousseeuw for LMedS scale estimation ([18], p.202). The amount of underestimation is significant for small k, which is a positive artifact since it compensates for small sample size effects in computing (3). The underestimation decreases monotonically with increasing k. Given the stochastic nature of the processes, all the properties should be regarded as true with high probability.

For homogeneous data, $\hat{\sigma}_k^2$ is the unbiased sample variance of the noise (3), and therefore it is close to σ^2 once k is large enough. Thus, the criterion (3) compares a nonrobust and a robust estimate of the noise variance. Since $\hat{\sigma}_k^2$ (belonging to the least squares family of estimators) is more efficient than $\hat{s}_k$, the underestimation of σ by the latter is the predominant effect till large k values. For homogeneous regions the criterion (3) has its minimum for larger k-s, and almost all data points are classified as inliers.

Let us now consider nonhomogeneous data. The $n - m$ inliers are corrupted with i.i.d. zero-mean noise having standard deviation σ, and the remaining m points are outliers. The inliers provide the largest homogeneous region, but can represent only a relative majority in the data. The outliers can be structured as well, as is the case in the piecewise polynomial surface approximation of range images.

First $k \leq n - m$. Assume that the LKS estimator returns an unbiased estimate of the model for the inliers. This always can be achieved by using enough p-tuples. It is important to recognize that the residuals of the $n-m$ inliers are distributed *over the entire range* of the noise. As k increases (but remains less or equal than $n - m$) the estimate $\hat{s}_k$ increases monotonically since residuals significantly larger than σ are used in (1). The phenomenon, an artifact of the data nonhomogeneity, was analyzed in details in [15] and can cause high breakdown point

estimators to loose their robustness properties for low signal-to-noise ratios. Thus it is expected that for $k \leq n - m$ the criterion (3) decreases monotonically as k increases. The observation was verified by extensive simulations. Once $k > n - m$, at least one data point in the window is an outlier and the estimated model is never correct. Most of the $n - m$ residuals of the inlier points increase significantly, yielding an increase of the criterion (3).

As a simple example consider a noisy step edge analyzed under the linear (planar) model. When $k \leq n - m$ the residuals of the inlier points are bounded by the noise, i.e., $\mid r_{i,k} \mid < 2.5\sigma$. When $k > n - m$ and the noise is significant, the linear fit bridges across the step and the same points have now a linear error term added to their residuals yielding a large jump in the value of $\hat{\sigma}_k^2$. For normal noise and $k \leq n - m$ the estimate $\hat{\sigma}_k^2$ is χ^2 distributed, while when $k > n - m$, obeys a noncentral χ^2 distribution whose mean is increased with the noncentrality parameter of the distribution ([16], p.42).

The estimate $\hat{s}_k$ is also corrupted when the window of analysis (1) contains outliers. However, the increase of $\hat{s}_k$ is much less than that of $\hat{\sigma}_k$ since only the difference of two residuals and not their squared sum is used. Thus, once k exceeds the size of the inlier region, the criterion ϵ_k^2 is expected to increase significantly. A theoretically possible failure is worth mentioning. If several extreme outliers are present in the data, $\hat{s}_k$ can become so large that the minimum of the criterion is produced at an incorrect k. However, for real data the pixel domain is bounded and such a situation cannot happen.

The above qualitative analysis also shows one of the limitations of the criterion (3). If, for values of k just exceeding $n - m$ the change in the structure of the residuals is not very abrupt, the criterion may not yield the minimum at the correct k. In the noisy step-edge example it happens when the signal-to-noise ratio, the step height relative to σ, is small [15]. More complex piecewise surfaces (like a roof edge, or a double step) are more prone to errors since there are more data points close to an erroneous fit. The "bridging fits problem" of the robust estimators [21], [22] is another aspect of the same phenomenon. As will be shown below, the

ALKS procedure is less sensitive but not immune to adverse conditions.

To compare the performance of ALKS with that of other estimators, least squares (LS), LMedS, MINPRAN and RESC, four piecewise linear one-dimensional synthetic signals of increasing complexity were generated. Each signal contained 100 data points corrupted with zero-mean, i.i.d. Gaussian noise having standard deviation σ. A percentage α of the data points was also corrupted with impulse noise uniformly distributed in the range of $(0,\ \ 100)$.

Line. Points (1–100): $y = x - 1$. $\sigma = 5$. $\alpha = 0.5$.

Step. Points (1–55): $y = 30$; (56–100): $y = 60$. $\sigma = 3$. $\alpha = 0.2$.

Roof. Points (1–55): $y = x - 1$; (56–100): $y = 109 - x$. $\sigma = 2$. $\alpha = 0.2$.

Double-step. Points (1–40): $y = 20$; (41–65): $y = 40$; (66–100): $y = 60$. $\sigma = 1$. $\alpha = 0.1$.

In Fig. 1 the four signals are shown. The ALKS procedure used 500 p-tuples for each value of k. This number can be reduced significantly without performance deterioration. Also, similar to [9], the same samples can be used for different k-s. Only the multi-step procedures RESC and ALKS show correct results across all the cases. However, RESC requires user tuned parameters for optimal performance, while ALKS is entirely data driven.

The behavior of the ALKS estimator is shown in Fig. 2. Nineteen uniformly spaced values of the index $\eta = k/n$ were defined between 0.05 and 0.95. The four signals were generated 1000 times and the ALKS procedure was applied to recover the largest homogeneous region. In Fig. 2a the dependence of ϵ_k^2 on the index η, averaged over the 1000 trials, is shown. The minimum of ϵ_k^2 is always close to the percentage of the largest homogeneous region in the signals. Note how the steepness of the change depends on the structure of the signal. The change is least abrupt for the *roof* signal where the transition between the two regions is continuous. The probabilities of detection are shown in Fig. 2b. The spread of the significant probability values is small and thus the recovery of the largest homogeneous region is robust.

3 Range Image Segmentation with ALKS

The ALKS procedure can be used as the computational module for a robust range image segmentation algorithm. Since the ALKS estimator detects the relative majority the algorithm can start by defining the first processing window as the entire image. This eliminates the need for heuristic procedures often involved in finding the seed regions.

The order of the polynomial surface used as model is an important consideration in range image analysis: planar, quadratic or cubic [4]. We have found that higher order surfaces can be accurately approximated when the segmentation is based only on planar surfaces, but uses high breakdown point estimators. If necessary, the planar patches then can be fused using the adequate model order. The increased number of degrees of freedoms of a higher order model often can yield undersegmentation artifacts. For example, a spatial roof edge (a crease) will be fused under a quadratic surface model. The only systematic study of the performance of range image segmenters [8] also used planar patches.

The ALKS based range image segmentation algorithm can be summarized as follows:

1. Define the region to be processed as the largest connected component of unlabeled pixels. At the start, this means the entire image. The connected component algorithm from [7], vol. 1, Sec. 2.3.5, was used.

2. Apply the ALKS procedure to the selected region and discriminate the inliers.

3. Label the largest connected component of inliers as the delineated homogeneous patch.

4. Refine the model parameter estimates by a least squares fit to the inliers.

5. Repeat steps 1–5 till the size of the largest connected component is less than a threshold (100 pixels was used in the implementation).

6. Eliminate the isolated outliers surrounded by inliers. An unlabeled pixel is allocated to the class of the majority of its labeled four-connected neighbors.

The range image segmentation algorithm was tested on both synthetic and real 256×256 range images. The real images were captured by a range finder of the Seoul National University. The range finder uses the active triangulation method [17], and a resolution is 0.1 mm both for the interpixel distances and depth values. The raw images were interpolated with cubic surfaces to compensate for information loss due to shadow effects and nonlinear sampling along the row direction. The background and the objects have significantly different dynamic ranges, the former being automatically set to zero.

The first processing steps of the segmentation algorithm for a real range image are shown in Fig. 3. The original range image (Fig. 3a) has a restricted set of values between 7142 and 8242 (out of a total possible variation of 0 to 65535). The image was transformed into float representation and to emphasize the tolerance of the algorithm to missing data (outliers), was also corrupted with 10% impulse noise bounded only by the machine precision (-10^{30}, 10^{30}), (Fig. 3b). When applied to the entire image, the segmentation algorithm chooses the background as the first region (Fig. 3c). The next detected region is the largest one from the object (Fig. 3d). After a total of 9 iterations all the image is segmented. The labeled image (Fig. 3e) is shown before the impulse noise (isolated pixels) were removed. The reconstructed image (Fig. 3f) is close to the original, the mean square error is only 3.43 for 58784 pixels. (The remaining 6752 pixels are unclassified.) The segmentation (using 500 three-tuples per LKS iteration, and 19 steps for the index η) took less than 2 minutes on an Indigo 2 Silicon Graphics workstation.

In Fig. 4 the segmentation of three different range images are shown. Slightly distorted boundaries appear near the junction of surfaces, and the higher order surfaces are split into a number of planar patches. Note however, that the main boundaries of these objects are correct and thus, if needed, the quadratic surfaces can be recovered by further processing.

It is of importance to compare the performance of the algorithm with that of other robust range image segmentation methods. We have chosen three such methods. The first two are

typical for the spatial and feature space based approaches, and the third one is the already mentioned RESC technique [23].

As a robust segmentation method which emphasizes the spatial information provided by adjacent pixels, the robust region growing algorithm of Meer *et al.* [13] was implemented. The image was divided into nonoverlapping 15×15 blocks within which 7×7 windows were used for local processing. The algorithm starts by defining the inlier/outlier dichotomy for each block. At subsequent iterations the inlier regions are used as seed regions for the adjacent regions in a robust merging and/or outlier conquering procedure. All the other user set values of the algorithm were the same as in [13]. The dual approach toward segmentation is by clustering in the space of the surface parameters. Large homogeneous regions should yield well defined clusters in this space. The robust clustering technique described in [9] was implemented. A 15×15 window was used to locally estimate with an M-estimator the three parameters of the planar model. The other user set values were the same as in [9]. The implementation of the RESC technique followed the description in [23].

In Fig. 5 the results of these segmentation algorithms for the real range image in Fig. 3a are shown. For proper comparison small region elimination and merging procedures are not performed for any of the four methods. The black regions are pixels which did not acquire a label when the algorithm stopped. The region growing (Fig. 5a) and the RESC (Fig. 5c) algorithms show many incorrect regions near vertices or where the change of depth is very steep. The clustering algorithm (Fig. 5b) yields a large number of unlabeled pixels in the steep region as an artifact of the relative large window used in estimating the local parameters. The ALKS based algorithm (Fig. 5d) provides the most satisfactory segmentation results at a somewhat lower computational cost.

The performance evaluation work for range image segmentation algorithms [8] provides a large set of standard data together with the ground truth. We have used an image from the ABW family (Fig. 6a) whose segmentation ground truth is Fig. 6b. The results of two methods

analyzed in [8], the UB and USF algorithms with the parameters as described in the paper, are shown in Figs. 6c and 6d. They were taken from their web sites. The result for the ALKS segmenter is shown in Fig. 6e. There is one clear mistake in the segmentation, several faces of the right object are fused. However, this error can be recovered by further processing. The labels associated with the delineated regions are given in Fig. 6f. The mean square error of all the fits, except labels 5 and 8, were between 0.299 (label 10) and 0.914 (label 4). The remaining two labels had much larger fitting errors, 3.344 (label 5) and 5.298 (label 8). The latter is a region poorly captured by the sensor as the ground truth (Fig. 6b) also illustrates. The regions with high fitting errors can now be separated and thus analyzed with increased sensitivity. Since the goal of the comparison was to contrast the raw ALKS method with more traditional techniques, this processing step was not implemented. It must be emphasized, that the ALKS result is obtained without any user set tuning parameter (beside minimum region size) while the traditional methods require a search for the optimal set of thresholds [8].

4 Discussion

The adaptive least k-th order squares procedure described in this paper is designed to handle piecewise structured data, a case frequently met in computer vision. Its advantage relative to traditional techniques or similar multi-step robust procedures (like MINIPRAN or RESC) is its lack of embedded a priori assumptions. There are no parameters to be tuned for optimal performance, and the outliers can have arbitrary structure. While the inliers are assumed to be corrupted by normal noise, this hypothesis has practically no influence on the results as examples with real images have shown.

Inspired by an earlier version of the ALKS procedure, Stewart developed the MUSE (minimum unbiased scale estimator) technique [14]. The MUSE operator detects the homogeneous patch corresponding to a relative majority in the processing window, by seeking the value of

k for which the k-th ordered residual (normalized by the expected value of the corresponding order statistic of the standard residual distribution) is minimum. The MUSE technique puts the emphasis on the nature of the inlier distribution and requires a lookup table for the scale estimator correction. In the ALKS approach the optimal region size is determined by comparing a robust and a nonrobust estimate of the noise variance and not based on a single residual. Extensive theoretical analysis and simulations have shown [14] that MUSE will fail around signal-to-noise ratios at which the performance of MINIPRAN, ALKS or RESC also decline. For a step signal, this will appear close to a step height of 8σ.

Range image segmentation in particular, and robust analysis of image structures under the piecewise polynomial surface model in general, are difficult problems with the currently available solutions being not general enough to be able to handle arbitrary data. A possible way toward further progress is to overcome some of the inherent limitations of high breakdown point robust estimation techniques.

Acknowledgement

We would like to thank Chuck Stewart from Rensselaer Polytechnic Institute for discussions which significantly improved the initial version of the algorithm, Adam Hoover from University of South Florida for helping with the USF database, and Prof. S.U. Lee from Seoul National University for providing the range images. This work was supported in part by the Engineering Research Center for Advanced Control and Instrumentation (KOSEF), Seoul National University, Seoul, Korea. Peter Meer acknowledges the support of the National Science Foundation through the grant IRI-9210861.

References

[1] F. Arman and J. K. Aggrawal, "Model-based object recognition in dense-range images – A review," *ACM Computing Surveys*, vol. 25, no. 1, pp. 5–43, Mar. 1993.

[2] P. J. Besl, *Surfaces in Range Image Understanding*. New York: Springer-Verlag, 1988.

[3] P. J. Besl, J. B. Birch, and L. T. Watson, "Robust window operators," *Machine Vision and Applications*, vol. 2, pp. 179–192, 1989.

[4] K.L. Boyer, M.J. Mirza, and G. Ganguly, "The robust sequential estimator: A general approach and its application to surface organization in range data," *IEEE Trans. Pattern Anal. Machine Intell.*, vol. PAMI-16, no. 10, pp. 987–1001, Oct. 1994.

[5] T. J. Fan, G. Medioni, and R. Nevatia, "Segmented descriptions of 3-D surfaces," *IEEE Trans. Robotics and Automation*, vol. RA-3, no. 6, pp. 527–538, Dec. 1987.

[6] R.C. Bolles and M.A. Fischler, "A RANSAC-based approach to model fitting and its application to finding cylinders in range data," *Proc. 6th International Joint Conf. on Artificial Intelligence*, Vancouver, Canada, Aug. 1981, pp. 637–643.

[7] R.M. Haralick and L.G. Shapiro, *Computer and Robot Vision.*, Reading, MA: Addison-Wesley, 1992.

[8] A. Hoover, J.-B. Gillian, X. Jiang, P.J. Flynn, H. Bunke, D. Goldgof, K. Bowyer, D.W. Eggert, A. Fitzgibbon, R.B. Fisher, "An experimental comparison of range image segmentation algorithms," *IEEE Trans. Pattern Anal. Machine Intell.*, vol. PAMI-18, no. 7, pp. 673–689, July 1996.

[9] J.-M. Jolion, P. Meer, and S. Bataouche, "Robust clustering with applications in computer vision," *IEEE Trans. Pattern Anal. Machine Intell.*, vol. PAMI-13, no. 8, pp. 791–802, Aug. 1991.

[10] V. Koivunen and M. Pietikäinen, "Evaluating quality of surface description using robust methods," *Proc. 11th International Conference on Pattern Recognition*, The Hague, The Netherlands, Aug. 1992, **III**, pp. 214–218.

[11] A. Leonardis, A. Gupta, and R. Bajcsy, "Segmentation of range images as the search for geometric parametric models," *International Journal of Computer Vision*, vol. 14, no. 3, pp. 253–277, Apr. 1995.

[12] P. Meer, D. Mintz, D. Y. Kim, and A. Rosenfeld, "Robust regression methods for computer vision: A review," *Int. Journ. Computer Vision*, vol. 6, no. 1, pp. 59–70, Apr. 1991.

[13] P. Meer, D. Mintz, and A. Rosenfeld, "Least median of squares based robust analysis of image structure," *Proc. 1990 DARPA Image Understanding Workshop*, Pittsburgh, PA, Sep. 1990, pp. 231–254.

[14] J.V. Miller and C.V. Stewart, "MUSE: Robust surface fitting using unbiased scale estimates," *Proc. Computer Vision and Pattern Recognition '96*, pp. 300–306, San Francisco, CA, June 1996.

[15] D. Mintz, P. Meer, and A. Rosenfeld, "Consensus by decomposition: A paradigm for fast high breakdown point robust estimation," *Proc. 1991 DARPA Image Understanding Workshop*, La Jolla, CA, Jan. 1992, 345–362.

[16] J.G. Proakis, *Digital Communications.* Third edition. New York: McGraw-Hill, Inc, 1995.

[17] M. Rioux, "Laser range finder based on synchronized scanners," *Applied Opt.*, vol. 23, no. 21, pp. 3837–3844, 1984.

[18] P. J. Rousseeuw and A. M. Leroy, *Robust Regression and Outlier Detection*. New York: John Wiley & Sons, 1987.

[19] P. J. Rousseeuw and C. Croux, "Alternatives to the median absolute deviations," *Journal of the American Statistical Association*, vol. 88, pp. 1273–1283, Dec. 1993.

[20] G. Roth and M.D. Levine, "Extracting geometric primitives," *CVGIP: Image Understanding*, vol. 58, no. 1, pp. 1–22, July 1993.

[21] C. V. Stewart, "Expected performance of robust estimators near discontinuities," *Proc. Fifth International Conf. on Computer Vision*, pp. 969–974, Boston, MA, June 1995. Revised version to appear, *IEEE Trans. Pattern Anal. Machine Intell.*

[22] C.V. Stewart, "MINPRAN: A new robust estimator for computer vision," *IEEE Trans. Pattern Anal. Machine Intell.*, vol. PAMI-17, no. 10, pp. 925–938, Oct. 1995.

[23] X. Yu, T. D. Bui, and A. Krzyzak, "Robust estimation for range image segmentation and reconstruction," *IEEE Trans. Pattern Anal. Machine Intell.*, vol. PAMI-16, no. 5, pp. 530–538, May 1994.

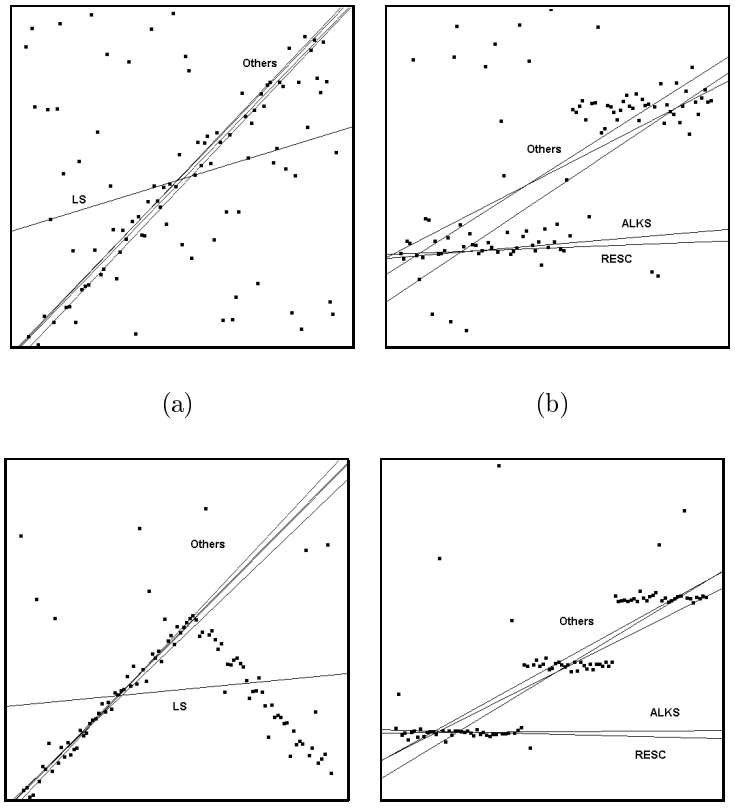

(a) (b)

(c) (d)

Figure 1: Comparison of five line fitting methods. See text.

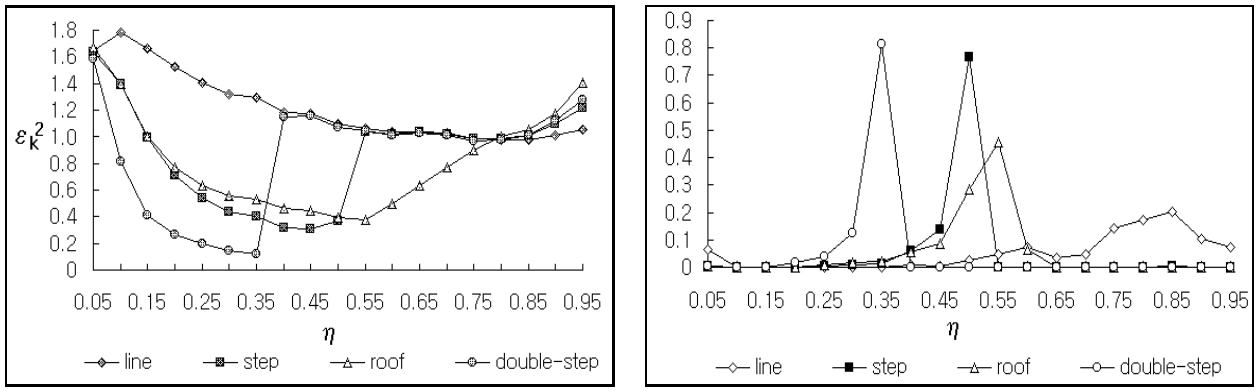

(a) (b)

Figure 2: Performance analysis of the adaptive LKS. (a) Dependence of the optimality criterion on the index. (b) Probabilities of detection.

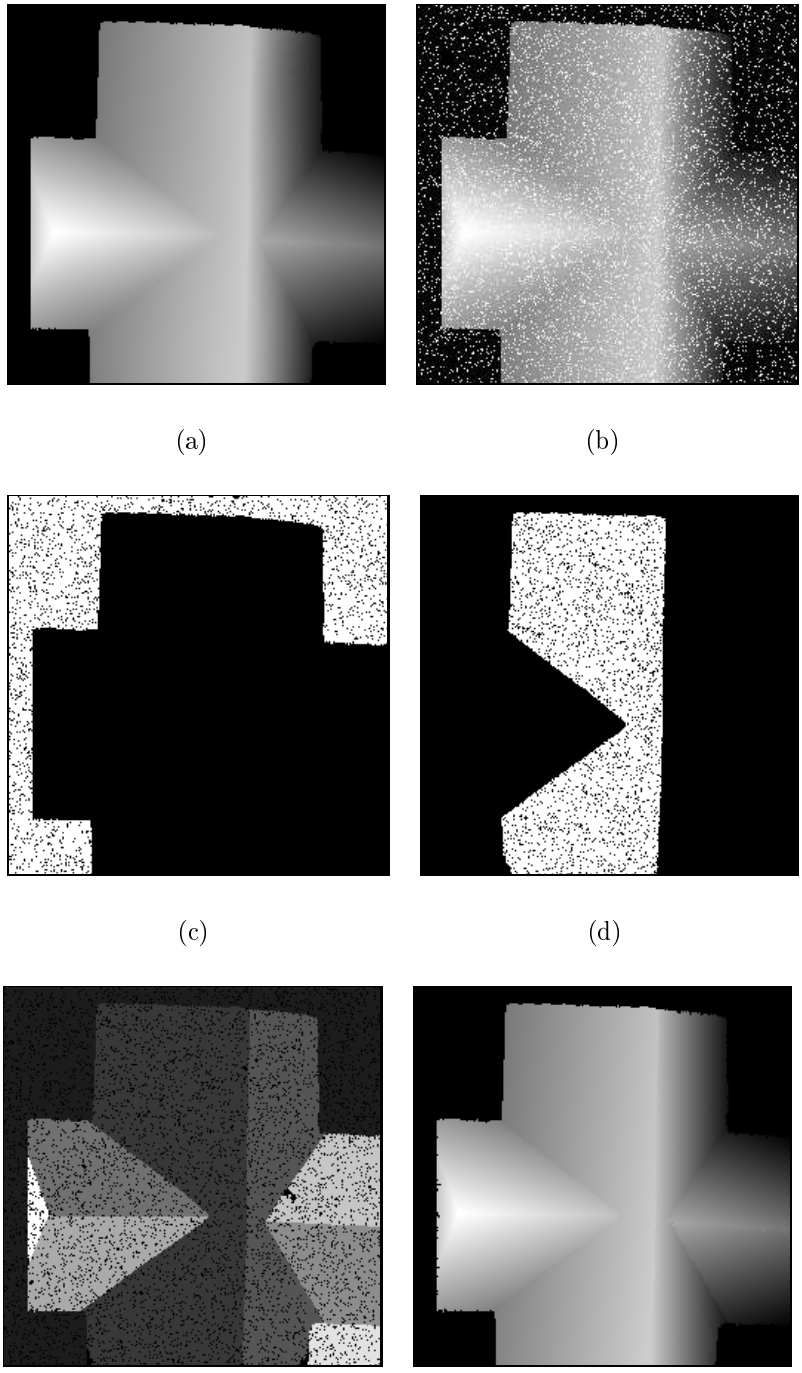

Figure 3: Processing of a range image. (a) Original image. (b) Noisy image. (c) First region detected (the black region is not processed at this iteration). (d) Second region detected. (e) Labeled image (impulse noise retained). (f) Reconstructed image (impulse noise removed).

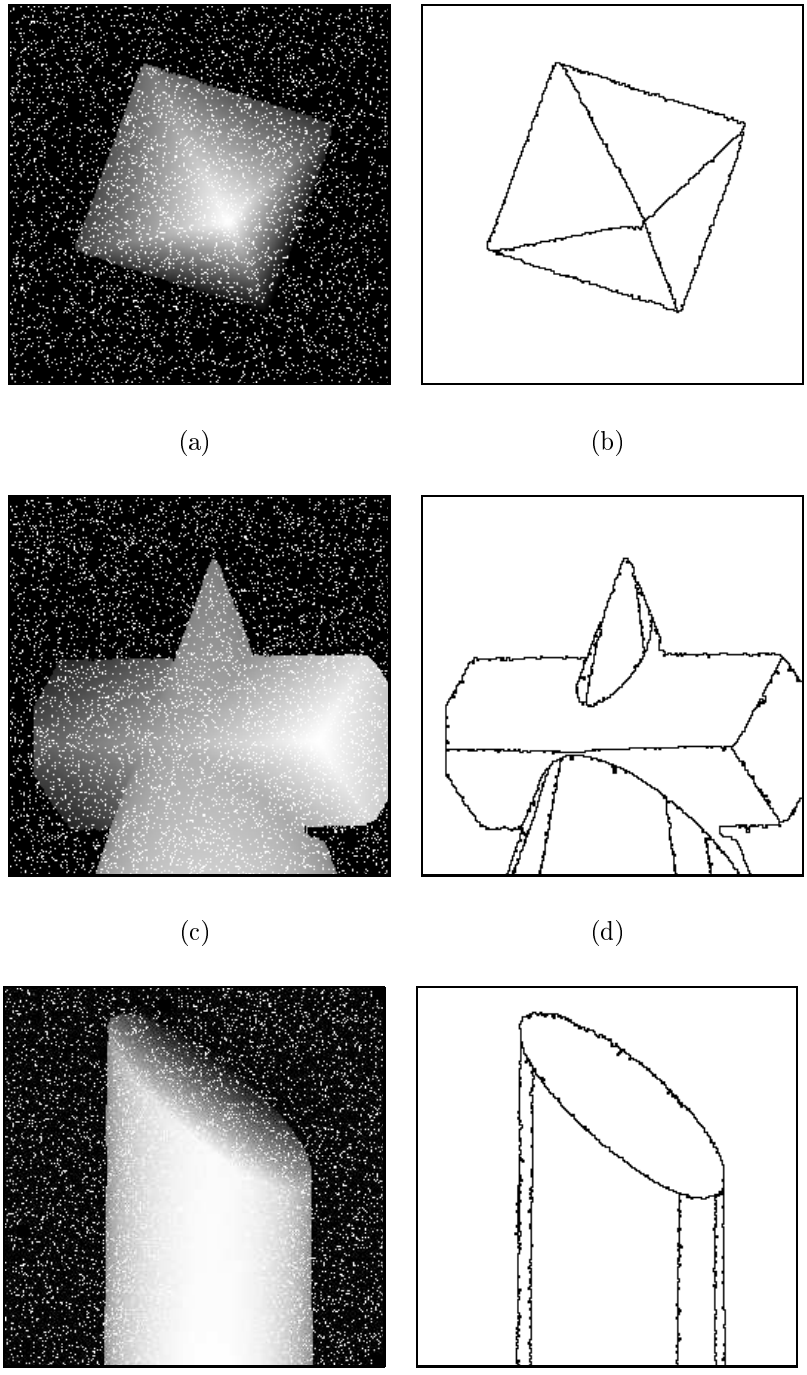

(a) (b)

(c) (d)

(e) (f)

Figure 4: Segmentation of three real range images corrupted with impulse noise.

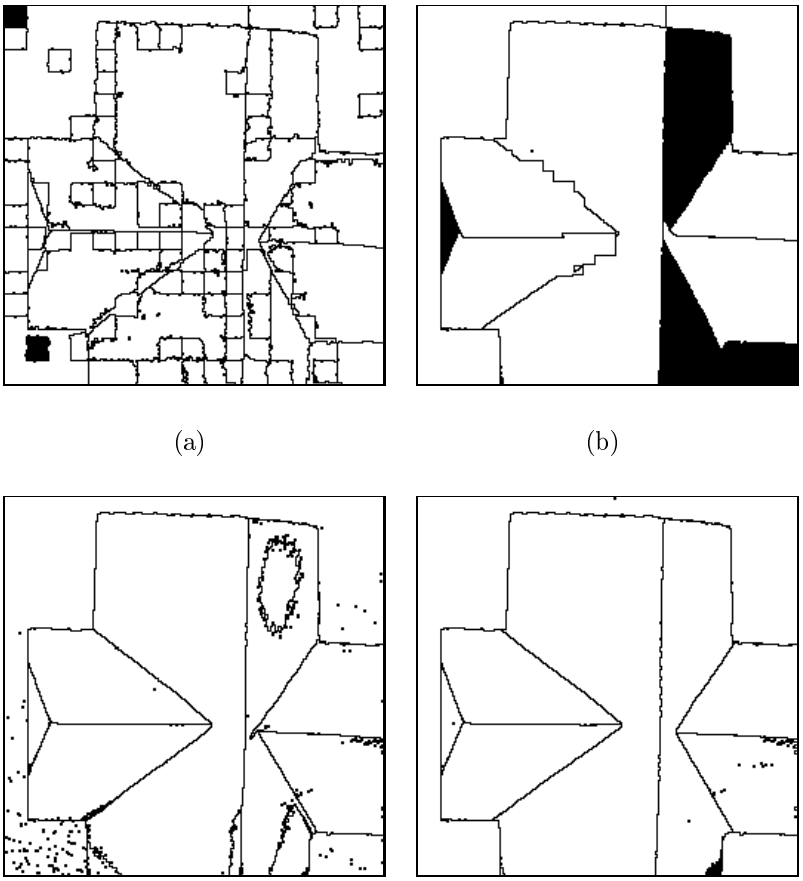

(a) (b)

(c) (d)

Figure 5: Comparison of segmentation results for the real range image in Figure 3a. (a) Meer *et al.* (b) Jolion *et al.* (c) Yu *et al.* (d) ALKS.

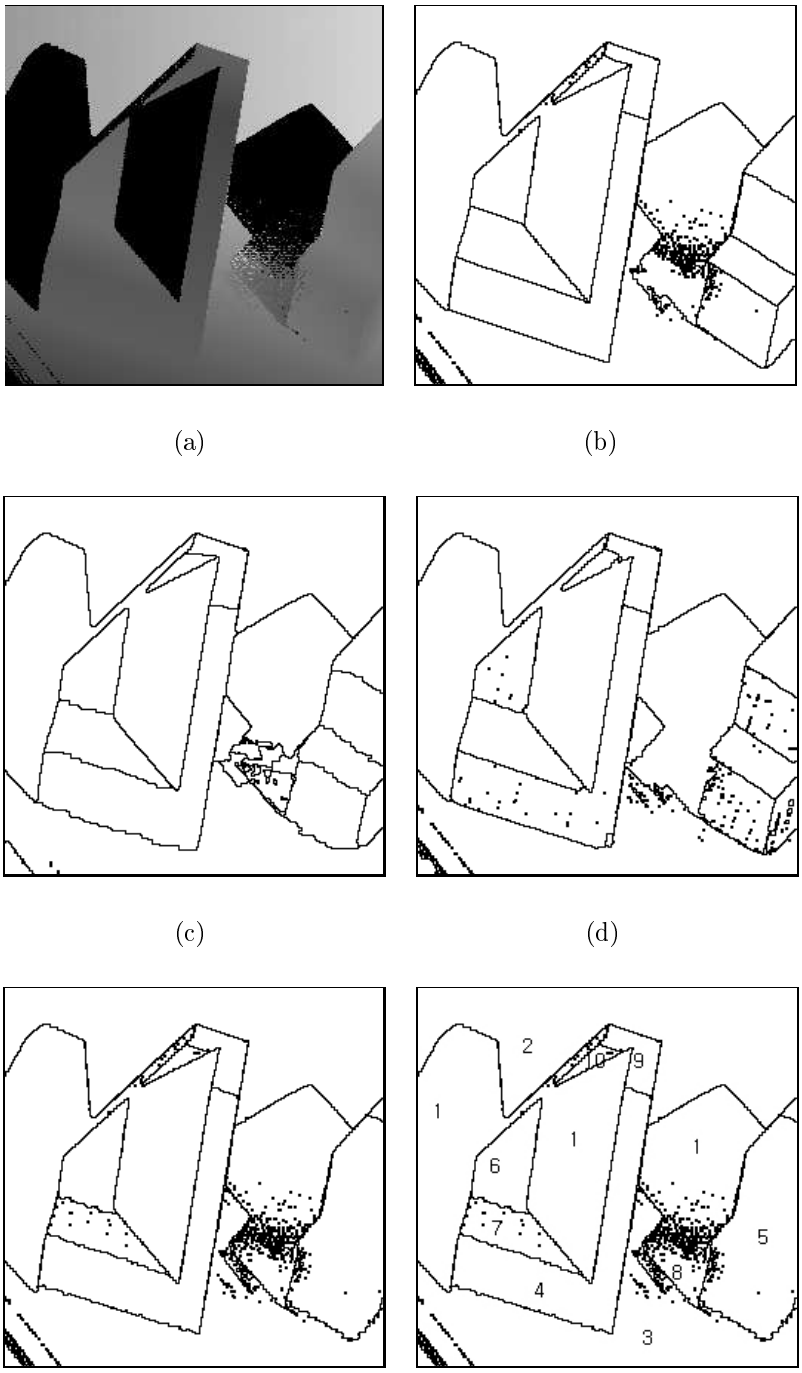

Figure 6: Comparison of the segmentation results for the ABW image from the USF database. (a) Range image. (b) Segmentation ground truth. (c) Result of the UB algorithm. (d) Result of the USF algorithm. (e) Result of the ALKS algorithm. (f) Label allocation in the ALKS result.